Charge density at the Al_2O_3/Si interface in Metal-Insulator-Semiconductor devices: semiclassical and quantum mechanical descriptions

© Slah Hlali, Neila Hizem, Adel Kalboussi

Laboratoire de Microélectronique et Instrumentation (LR13ES12), Faculté des Sciences de Monastir,
Avenue de l'environnement, Université de Monastir, 5019 Monastir, Tunisie

E-mail: hlalislah@yahoo.fr

(Received 3.02.2016. Received after revision 31.01.2017)

In this paper, a quantum correction computation of the inversion layer of charge density was investigated. This study is carried out for a one-dimensional Metal-Insulator-Semiconductor (MIS) structure with (100) oriented P-type silicon as substrate. The purpose of this paper is to point out the differences between the semiclassical and quantum-mechanical charge description at the interface Al_2O_3/Si, and to identify some electronic properties of our MIS device using different thickness of the high-k oxide and diverse temperature with different carrier statitics (Fermi–Dirak statitics and Boltzmann statitics). In particular, the calculations of capacitance voltage ($C-V$), sheet electron density, a relative position of subband energies and their wave functions are performed to examine qualitatively and quantitatively the electron states and charging mechanisms in our device.

DOI: 10.21883/FTP.2017.12.45185.8190

1. Introduction

In accordance with Moore's law, the gate oxide thickness must be reduced in order to maintain an acceptable scaling of MOS transistor dimensions. Caused by the occurrence of high level direct tunneling currents, we are approaching the limits in reducing silicon dioxide (SiO2) gate thickness [1]. Future CMOS technology nodes will require the introduction of alternative high-k dielectrics such as aluminum oxide, hafnium oxide (Al_2O_3, HfO_2, etc.), which appear at present as the most serious candidates. In order to get the high density integration of MOS devices, it is obligatory to reduce the gate oxide thickness and to increase the substrate doping concentration. This results in a narrow and deep potential well in which electrons are confined at the semiconductor-insulator interface, and it becomes necessary to take a quantum mechanical (QM) effects into consideration [2].

Under such conditions, quantum effects in the inverted channel of MOSFET become important and strongly influence the device behavior and performance [3]. Modeling of MOS devices is usually performed by using drift diffusion algorithms, and much work on the classical model has been described in [4,5]. Several commercial simulators based on such classical approach exist. According to the National Technological Roadmap for semiconductors (NTRS) [6], Metal/high-k gate stacks have been implemented in the most recent technology generation in order to allow scaling of the EOT, consistent with the overall transistor scaling while keeping gate leakage currents within tolerable limits. The scaling tendency for gate dielectrics is such that for the sub-100 nm generation device, an equivalent gate oxide thickness of less than 3.0 nm will be required [7]. The combination of thin gate dielectric and high level gate bias results in a deep submicron ($< 0.25\,\mu$m) MOS device in large transverse electric fields at the interface. When the transverse electric fields become large enough to cause the formation of a 2D electron (or hole) gas, the modeling of quantum mechanical (QM) effects becomes very important. In this context, the consideration of quantum effects has been carried out by a one-dimensional solution of the Schrodinger equation on a section of the channel perpendicular to the gate contact [8,9], but not precise enough to predict the performance of nano-devices [10]. At the nanometer size, highly developed tools are necessary to describe the wave nature of electrons and cover quantum effects like energy quantization.

In this paper, quantum correction in the calculation of the inversion layer of the charge density calculation has been studied. Calculations are carried out for the 1D Metal-Insulator-Semiconductor MIS structure with (100) oriented P-type silicon as substrate. The maximum oxide thickness T_{ox} is 1 nm, and a uniform doping profile is used for the silicon layer. The Fermi–Dirak distribution and the standard effective-mass approximation in a parabolic band are assumed. In what follows, we will describe the operation of MOS capacitors by assuming both the semiclassical and quantum-mechanical charge distribution. When the charge is treated semiclassical, only 1D Poisson equation needs to be solved. When the charge in the triangular quantum well is treated quantum-mechanically, a self-consistent solution of the 1D Poisson and Schrodinger equations has to be found.

The objective of this paper is to examine some basic concepts for MOS capacitors and to point out the differences between the semiclassical and quantum-mechanical charge description at the interface. With this example, we will examine the MIS capacitor with the following properties: the gate is made of metal with a work function equal to the silicon affinity, the oxide is a high-k material (Al_2O_3) and with P-type silicon as substrate.

In this context, we have studied some electronic properties of our MIS device in a semiclassical and quantum-mechanical charge description by using different thickness of the oxide and temperature with different carrier statitiks (Fermi–Dirak statitics and Boltzmann statitics). In particu-

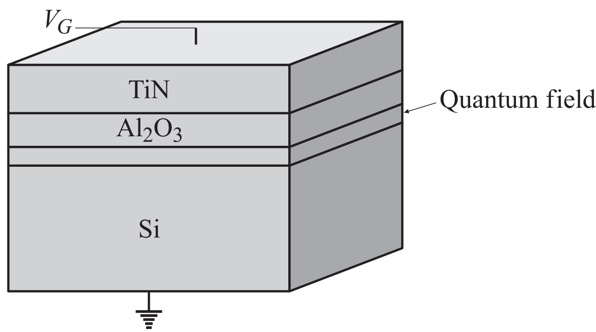

Figure 1. The structure of MOS capacitor.

lar, the capacitance voltage ($C-V$), the relative position of the subband energies and their wave functions are used to examine qualitatively and quantitatively the electron states and charging mechanisms in our structure. While most of the published studies on similar systems concentrate mainly on the $C-V$ measurements, here the energies, wave functions and sheet electron density data are highlited, which are found to be more sensitive to some aspects of carrier exchange mechanisms, and acquires additional information that could not be accessed through capacitance measurements alone.

2. Physical Model of 1D MOS Capacitor and their characteristic

1D MOS capacitor consists of three layers: metal, Al_2O_3 layer (oxide) and Si layer as shown in Fig. 1. QM effects are clear at the beginning of the Si layer.

Good addition of the quantum-mechanical size quantization effects in device simulators are achieved by solving the Schrodinger–Poisson–Boltzmann problem. This approach was discussed in details in [11]. Here we just focus on solving the 1D Schrodinger–Poisson problem for the correct description of charge quantization in MOS capacitors. This can be achieved with SCHRED First Generation tools, which are installed on the Network for Computational Nanotechnology.

The periodic crystal potential in the bulk of semiconducting materials is such that, for a given energy in the conduction band, the allowed electron wave vectors trace out a surface in a k-space. In the effective-mass approximation for silicon, these constant energy surfaces can be visualized as six equivalent minima of the bulk silicon conduction band split into two sets of subbands. One set consists of two equivalent valleys, which have the longitudinal mass perpendicular to the interface.

3. Results and discussion

We first illustrate $C-V$ characteristics by comparing the semiclassical and quantum mechanical model, in Fig. 2, our simulated results for low-frequency curves in one layer gate stacks with a p-doped Si substrate.

Fig. 2 shows the $C-V$ characteristic of simulations with quantum and semi-classical approach to our structure Metal/Al_2O_3/Si. We can see that in the quantum model, the simulated capacity is smaller than the capacity the semiclassical model and this is due to taking into account of the thickness of the darkspace. The zone of the darkspace is clearer in Fig. 3.

The low-frequency $C-V$ curve goes from accumulation through depletion toward inversion mode. Note that the threshold voltage for the semiclassical model is ~ -0.1 V, assuming that the minimum in the capacitance means the maximum in the threshold voltage. For the quantum mechanical model it is ~ 0 V; therefore the use of the quantum model gives rise to a threshold voltage shift of about 100 mV, which is a significant and physically justified

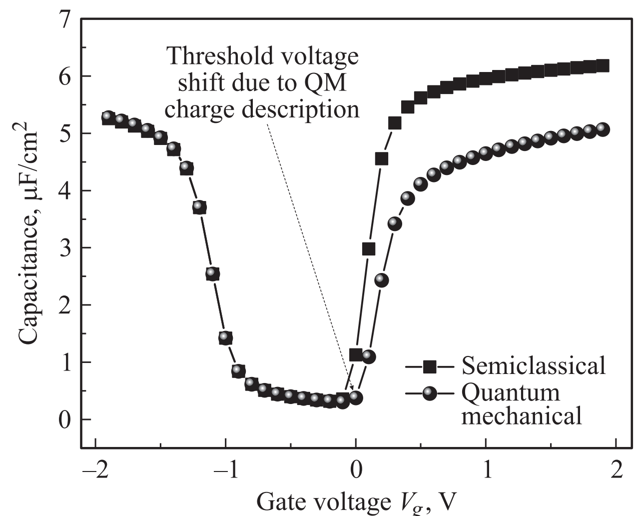

Figure 2. Capacitance versus voltage in the case of the semiclassical model (black) and the quantum model (red).

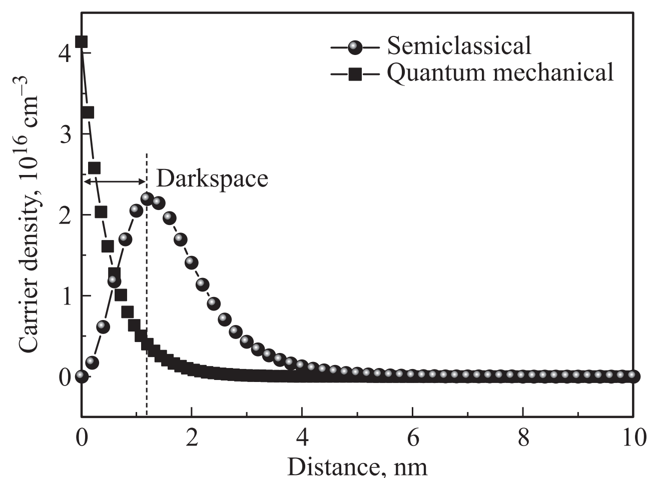

Figure 3. Semiclassical (squares) and quantum mechanical (circle) electron density. In this case, the deserted area carriers to „darkspace“ interface is illustrated.

value. During inversion, there is about 10% degradation of the total gate capacitance when using the quantum-mechanical model [12].

Throughout inversion, the capacitance degradation is almost constant, because our gate is a metal; this degradation can be accounted for via effective oxide thickness $T_{\text{eff}} > T_{\text{ox}}$. This degradation in inversion conditions has a manifest gate voltage dependence, and the total gate capacitance C_{tot} decreases with increasing V_G, when the gate is a poly-silicon.

We noticed from the curve 2 that the difference between the semiclassical model and the quantum-mechanical model is clear only in the inversion zone. This connected directly to the type of the substrate doping. In our case, the substrate is p-doped, so electrons are treated quantum mechanically only in the inversion area for positive voltages. We go further processing $C-V$ characteristics for the semiclassical and quantum models in the case of PMOS and NMOS for different oxide thickness values ranging from 0.3 to 1 nm.

The total charge density calculated semiclassically and quantum-mechanically at final bias $V_G = 2\,\text{V}$ is shown in Fig. 3. We examine that since the semiclassical electron density varies exponentially with the potential, as well as since the potential energy is the smallest at the interface, the peak density of semiconductor electrons is toward the Al_2O_3/Si interface decreases exponentially when the movement is toward the mass of the semiconductor. On the other hand, the quantum-mechanical electron density vanishes at the Al_2O_3/Si interface because of the large barrier. The peak of the electron density is away from the interface, which means that the average distance of the carriers increases for the quantum-mechanical case. The peak area between the carriers and the interface Al_2O_3/Si is depleted of carriers. This area is called „darkspace“, and can be modeled as an extra contribution to the effective gate oxide thickness [13,14]. The equations of the average distance of the carriers from the Al_2O_3/Si interface $(x = 0)$ for the semiclassical and quantum mechanical case, is given, respectively, by

$$Z_{av} = \frac{\int_0^\infty z n(z) dz}{\int_0^\infty n(z) dz} \quad \text{Semiclassical,}$$

$$Z_{av} = \frac{\sum_i N_i z_i}{N_s}, \quad \text{where}$$

$$z_i = \frac{\int_0^\infty z \psi_i^2(z) dz}{\int_0^\infty \psi_i^2(z dz)} \quad \text{Quantum mechanical,}$$

by N_i is denoted the sheet density in the i-th subband, N_s is the total sheet density and $\psi_i(z)$ is the i-th subband wave function.

The typical distance of the carriers is larger in the quantum mechanical case, this leads to a diminution of the inversion layer capacitance in addition to degradation of device trans-conductance.

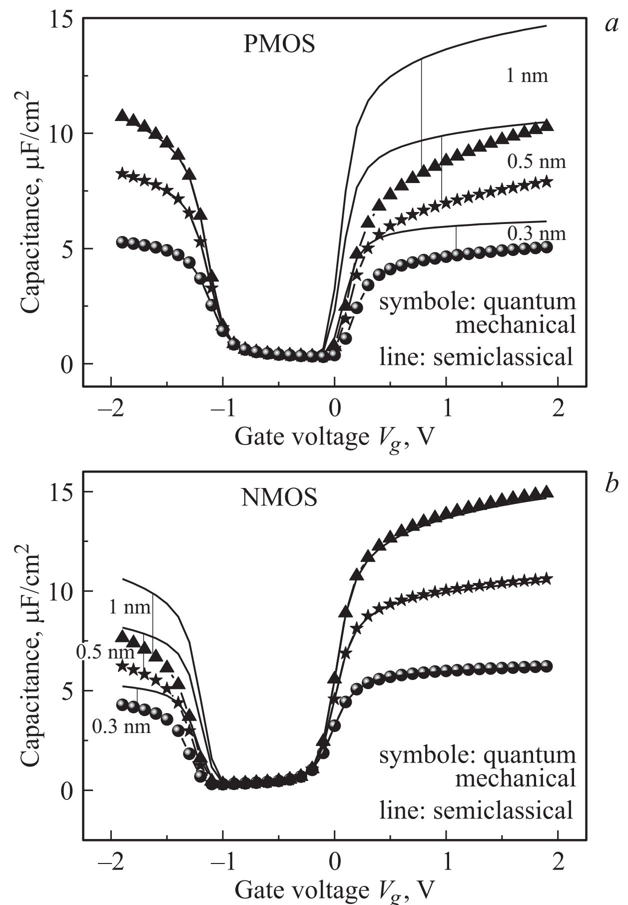

Figure 4. Capacitance versus gate voltage when using the semiclassical charge model (thin line) and quantum mechanical charge model (thick line). (a) for PMOS and (b) for NMOS.

As shown in Fig. 4, similarly to single-gate capacitors, the use of the quantum model leads to increase of the average distance of carriers from the interface and degradation of the total gate capacitance for positive gate bias.

In the case where there is a PMOS structure, it is noted that the quantum phenomenon on the $C-V$ characteristic belongs only to the inversion area for positive voltages. As a result, if the bulk is p-type silicon in the inversion range, electrons are treated quantum mechanically. Whereas in the accumulation range (NMOS: Fig. 4, b), holes are treated quantum mechanically. This is a feature, which many other simulators does not possess.

Therefore, shrink in gate oxide thickness promotes the use of the quantum well model. Indeed, for a low oxide thickness, the quantum effect becomes more and more significant. For that reason, a very high electric field reigns on the interface Al_2O_3/Si. The energy bands of the conduction and valence band near this interface, confining the carriers in a potential well, perpendicular to the plane of the interface. This causes a quantum confinement phenomenon quantization of energy carriers at discrete

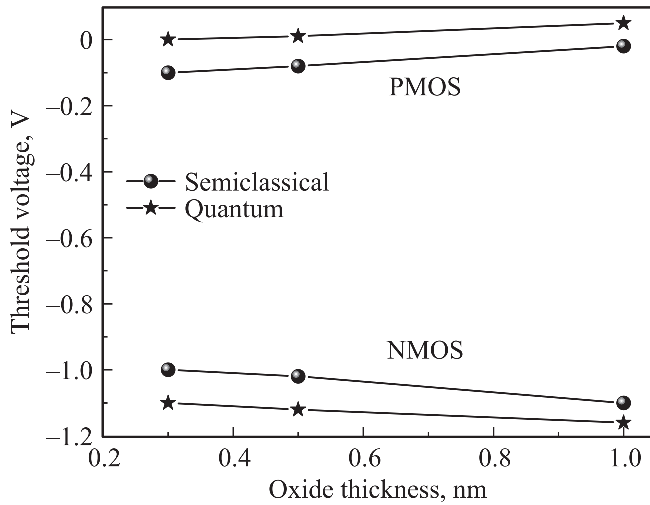

Figure 5. Variation of threshold voltage versus oxide thickness in the semiclassical and quantum model for PMOS and NMOS device.

levels. This is regarded as a 2D gas as mentioned by Scott et al. [15].

In the following Fig. 5, we have studied the variation of the threshold voltage, as a function of gate oxide thickness in the semiclassical and quantum mechanical case for both the PMOS and NMOS structures.

We noticed that the threshold voltage increases with increasing the oxide thickness of the PMOS structure both in the quantum and semi-classical case. Whereas, for the NMOS structure this voltage decreases with increasing oxide thickness. This threshold voltage shift must be taken into account in the design of ultra thin body device [16]. Therefore, the classical threshold condition, $\psi_s = 2\psi_B$, should be modified to $\psi_s = 2\psi_B + \Delta\psi_s^{QB}$ as mentioned by Cheon-Hakku et al. [17], where

$$\Delta\psi_s^{QM} = \frac{KT}{q} \ln\left(\frac{Q_i(\psi_s = 0)}{Q_i^{QM}(\psi_s = 0)}\right) \tag{1}$$

and Q_i is the total inversion charge density per unit area and is expressed in the classical manner as

$$Q_i = \frac{KTn_i^2}{E_s N_{\text{body}}}, \tag{2}$$

E_s is the electric field on the interface given by $E_s = \frac{qN_{\text{body}}T_{si}}{\varepsilon_{si}}$, and N_{body}, it is the doping concentration at the edge of the depletion layer Q_i^{QM}, is the total inversion charge corrected by quantum confinement per unit area and is expressed as:

$$Q_i^{QM} = \frac{4\pi qKT}{h^2}\left(gm_d \sum_j \ln\left(1 + e^{\frac{E_f - E_c' - E_f}{KT}}\right) + g'm_d' \sum_j \ln\left(1 + e^{\frac{E_f - E_c' - E_f}{KT}}\right)\right), \tag{3}$$

where g and g' are the degeneracy factors, m_d and m_d' are the densities of states of effective masses, $E_f - E_c'$ is the difference between the Fermi level and the bottom of the conduction band at the interface. Assuming that only the ground state is occupied by electrons, therefore the equation (1) becomes:

$$\Delta\psi_s^{QM} \approx \frac{E_0}{q} - \frac{KT}{q} \ln\left(\frac{8\pi qm_d E_s}{h^2 N_V}\right). \tag{4}$$

For NMOS, N_V is simply replaced by N_c, and the sign and the effective mass in Eq. (4) has changed. The ground energy state plays a crucial role in finding out the surface potential change by the quantum confinement effect. The ground energy state is powerfully prejudiced by the potential form. Finally, the expression of threshold voltage in the case of quantum mechanical model for PMOS and NMOS is given by:

$$\Delta V_{\text{th}}^{QM} = \frac{dV_g}{d\psi_s} \Delta\psi_s^{QM} = \left(1 + \frac{3T_{\text{ox}}}{T_{si}}\right)\left[\pm\frac{E_0}{q} \pm \frac{KT}{q} \ln\left(\frac{8\pi qm_d E_s}{h^2 N_c}\right)\right]. \tag{5}$$

In Fig. 6 we show the subband energies and the Fermi energy as functions of gate voltage in (100) silicon substrate from both unprimed (Δ2) and primed (Δ4) ladder of subbands. By this figure, we study two clearly pronounced characteristics. Here the triangular potential is narrowed, so elevated value for the subband energies and increased subband separation are obtained. By increasing the gate bias, we are touching into the electronic quantum limit. Consequently, most of the carriers will be staying in the ground subband of the unprimed (Δ2) ladder of subbands [12]. For (100) orientation of the interface, the carriers has the light mass in the transport direction and subsequently augments electron mobility.

Each of these subband energies, primed or unprimed, is described at the interface Al_2O_3/Si and more precisely

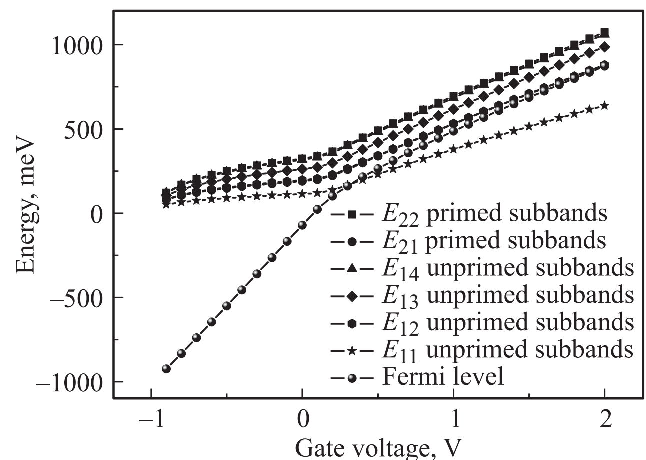

Figure 6. Relative position of the subband energies with respect to the Fermi level E_F as functions of the gate voltage.

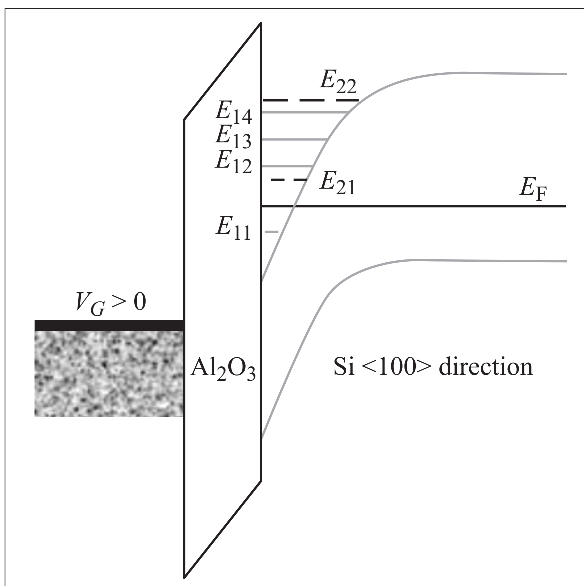

Figure 7. Potential diagram for inversion of p-type semiconductor. In this first notation E_{ij} (i : band, j = subband) refers to the j-th subbands from either the $\Delta 2$-band ($i = 1$) or $\Delta 4$-band ($i = 2$).

in the triangular quantum wells as exposed in Fig. 7. We observe that the Fermi-level is higher than the first subband for positive voltage. Hence, for that basis the semiconductor is degenerated. We notice also that as we go higher in energy, enlargement and the separation of energy levels becomes smaller and smaller.

In our case, for $\langle 100 \rangle$ orientation of the surface, the $\Delta 2$-band has the longitudinal mass (m_l) perpendicular to the semiconductor interface. Also, the $\Delta 4$-band has the transverse mass (m_t) vertical to the interface.

Fei Li [18] cited that if the channel potential could be approximated as an infinite triangular well. So, the substrate dielectric could be approximated as an infinite potential barrier in addition to the rise of the potential in the substrate. This rise is determined by the electric field at the interface. After that, the magnitudes of the bound-state energies comparative to the band edge might be obtained as

$$E_i \approx \left(\frac{\hbar^2}{2m^*}\right)^{\frac{1}{3}} \left[\frac{3}{2}\pi e E_s \left(i + \frac{3}{4}\right)\right]^{\frac{2}{3}}. \quad (6)$$

Using Airy functions with slight difference as compared to numerical calculations. Here, m^* is the quantization effective mass and i-labels the own state with $i = 0$ matching to the ground state.

In the case of the quantum-mechanical model we have taken 4 subbands from the unprimed ladder of subbands and 2 subbands from the primed ladder of subbands. The spatial deviation of the corresponding wave functions is shown in Fig. 8.

We can infer several important things that can be observed from the results shown in Fig. 8. The profile of the wave functions resembles Airy functions that are the solution to the 1D Schrodinger equations with linear potential energy term as mentioned by [19]. From Fig. 6 and 7 we detect that the minimum energy band in the quantum well primed or unprimed ladder of subbands correspond to the highest amplitude wavefunction. After that, if we compare the first two wave functions from both the unprimed and primed latter of subbands, we perceive that the unprimed wavefunctions are more squeezed as the energies are lower. Plus, for those energies, (see Fig. 6) the well is squeezed. For that reason, there exists larger localization of the carriers. We also noticed that the primary wave function has zero intersections with the x-axis, the second one has one, the third one has two, etc.

Fig. 9 shows the simulation of sheet electron density versus voltage curves of the MIS structure in both linear and semi-log (inset) scales. Here, we used two models semi-classical and quantum-mechanically to analyze and compare the tendency of electron density in our device for multi gate oxide thickness (1, 0.5 and 0.3 nm). We always notice whatever the oxide thickness, that sheet electron density in the semi-classical case is higher than that in the quantum-mechanically case. This can be explained by a bandgap enlargement in the case of the quantum-mechanical model

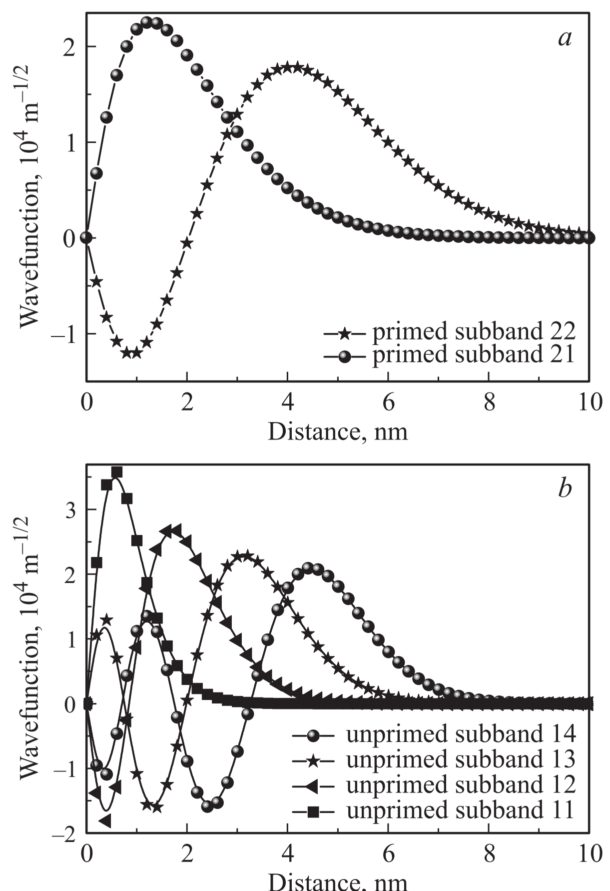

Figure 8. Wave functions corresponding to the lowest 2 subbands from the primed ($\Delta 4$) ladder of subbands (a), and wave functions corresponding to the lowest 4 subbands from unprimed ($\Delta 2$) ladder of subbands (b).

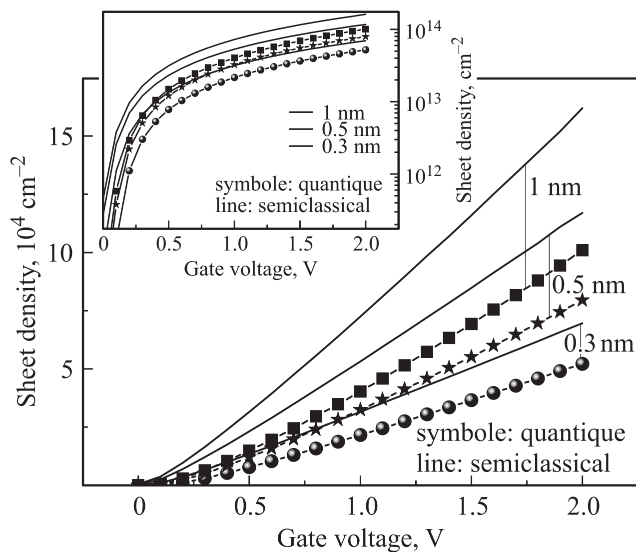

Figure 9. Sheet electron density in a semiclassical and Quantum mechanical model for different gate oxide thickness as a function of the gate voltage. Inset: semi-log behavior of sheet electron density.

due to the shift of the first tolerable state in the conduction band. Moreover, we can clarify too by the set-back of charge from the interface (seen from the results shown in Fig. 3), because the wave function vanishes right at the interface, which leads to effective oxide thickness bigger than the physical oxide thickness, hence leading to trans-conductance reduction. Each time, by reducing the thickness of the oxide, we note that the difference between the quantum and semi-classical curve increases.

We understand several important features. First, the electrons are more confined with rising the gate voltage and show smaller regular distance from the Al_2O_3/Si interface with increasing the gate bias. The contrary is correct for holes. Second, we examine that with increasing gate bias, electrons are more and more confined and the holes are not confined at all. The electron confinement increases with increasing positive gate bias because the quantum well becomes closer. As the carriers are in this case confined nearer to the interface, interface-roughness will begin to play a more important role and affect the bulk mobility, which is on the order of 1500 cm^2/V-s for bulk Si to inversion layer mobility on the order of 200 cm^2/V-s for the highest doped samples (smallest devices). This will have large implications on the transport characteristics of the device.

In what follows in Fig. 10, we will examine the variation of the capacitance as well as the sheet electron density in the semi-classical and quantum model case for different temperature values. Here we analyze our MIS device where the oxide has a 1 nm thickness, and the substrate having a doping value $1 \cdot 10^{18}$ cm^{-3}.

In Fig. 10, *a* we illustrate the effects of quantum mechanics on the semi-classical (low frequency) capacitance of a P-MIS capacitor as the gate bias varies at different temperature ranging from 50 to 450 K, taking the device from being in accumulation through to strong inversion. The main features are the shift in threshold voltage, equality of the capacitances near the flat band and in depletion, and the different asymptotic capacitance as the gate voltage becomes large for positive bias. For Fig. 10, *b* we have studied the behavior of sheet electron density at low, medium and high temperature for both semi-classical and quantum model. We notice that the effect of temperature is clear around 0 V. Whereas, at high bias between 1and 2 V there is no change appears (see the semi-log Fig).

In order to study the influence of carrier statitics type (Fermi–Dirak and Boltzmann statitics) in the semi-classical charge model on the $C-V$ behavior of our MIS device, we point up $C-V$ characteristics by comparing, in Fig. 11, the two carrier statitics model for low-frequency curves in three different *p*-doped substrate type Si, GaAs and InAs.

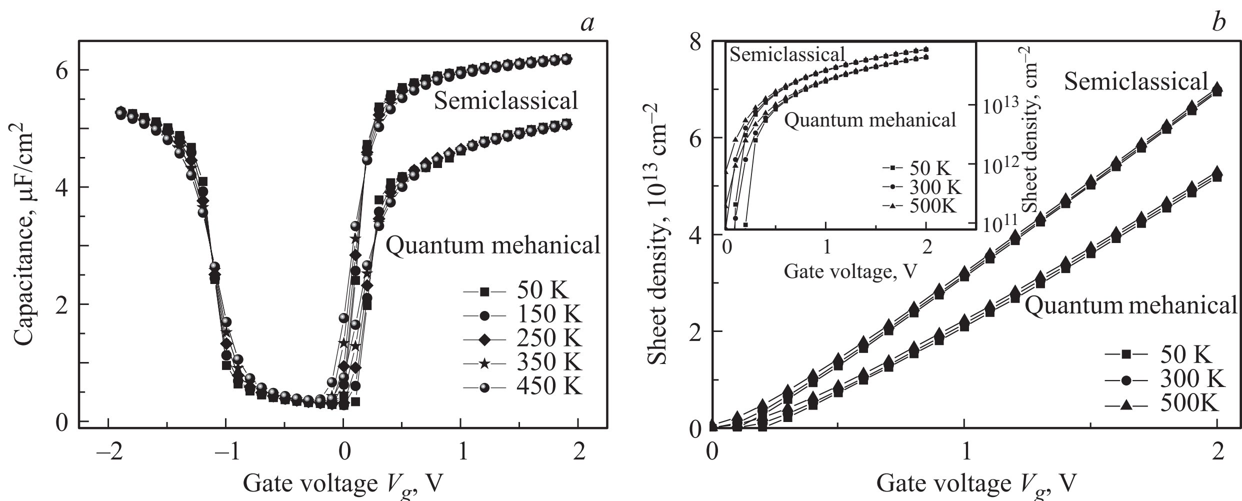

Figure 10. Capacitance (*a*) and sheet electron density (*b*) as function of gate bias at different temperature for both semiclassical and quantum mechanical model for the charge description. Inset in (*b*): semi-log tendency of sheet electron density.

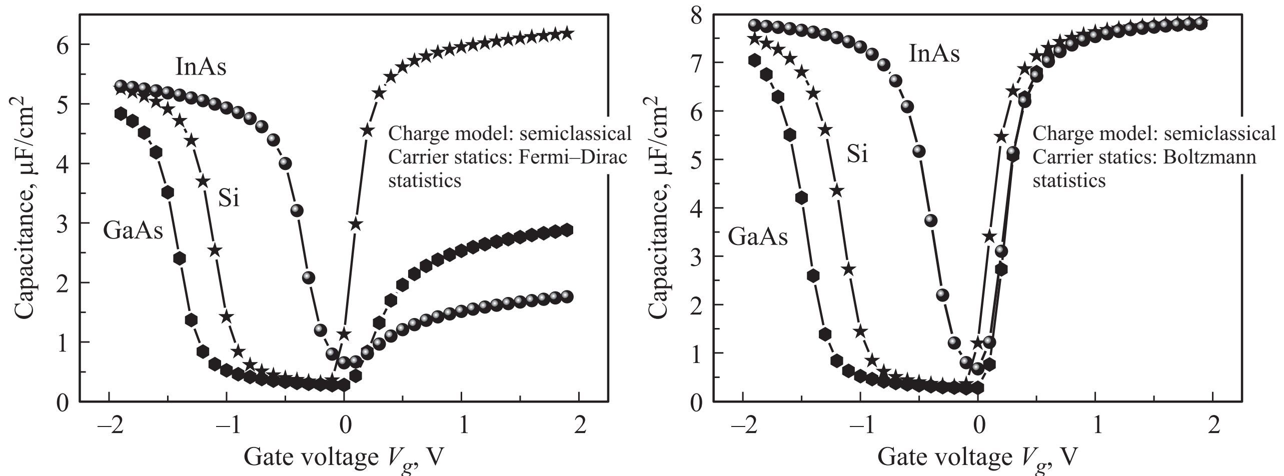

Figure 11. Simulated $C-V$ characteristics for three different p-doped semiconductors ($N_A = 1 \cdot 10^{18}\,\text{cm}^{-3}$) with an Al_2O_3 gate dielectric layer of 1 nm (EOT = 0.43 nm) and $\phi_M = 4.05\,\text{eV}$ (fixed for all structures).

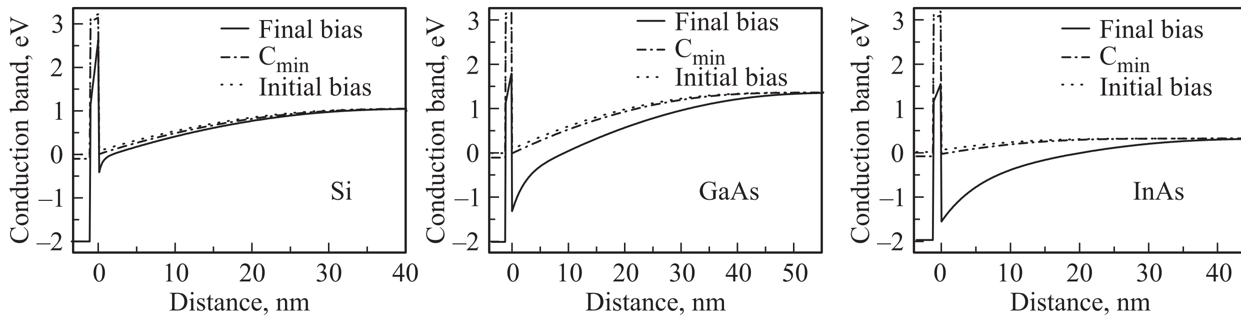

Figure 12. Conduction band profile in a MIS capacitor with a three p-type substrate (Si, GaAs and InAs) for initial, medium and final applied bias.

Fig. 11 compares simulation results for various Al_2O_3/III–V relative with Al_2O_3/Si materials MOS devices ($T_{Al2O3} = 1\,\text{nm}$, i.e. EOT = 0.43 nm) for which the gate work function is equal to 4.05 eV for all structures. The most important material parameters used in simulations are presented in table. It is important to remember that these constants (dielectric constant, effective mass, etc) strongly depend on the fabrication process and are not precisely known, particularly for dielectric materials. Thus, the values in the simulation code can be tailored in order to improve the fit between experimental and simulation results.

We can distinguish from Fig. 11 that the depletion zone strongly depends on the semiconductor bandgap. Furthermore, the very low effective density of state in the conduction band of III–V semiconductors is obviously evidenced in inversion regime, which leads to low capaci-

The main material parameters [20] of different semiconductors and dielectric materials used for our MIS device simulation. The band offsets between oxides and semiconductors are the same as in reference [21]

Materials	Physical Parameters (300 K)							
	E_g (V)	$\varepsilon/\varepsilon_0$	$m^*_{e,l}/m_0$	$m^*_{e,t}/m_0$	$m^*_{l,h}/m_0$	$m^*_{h,h}/m_0$	$m^*_{s,o}/m_0$	Band offsets for Al_2O_3 on each semiconductor
Si	1.12	11.8	0.916	0.19	0.20	0.291	0.29	2.6
GaAs	1.424	10.9	0.063		0.082	0.51	0.15	2.7
InAs	0.354	12.3	0.014		0.026	0.41	0.16	3.6
SiO_2	9.0	3.9	0.5					
Al_2O_3	6.1	9.0	0.35					

tance values in $C-V$ characteristics for Fermi–Dirak carrier statitics. We remark that in the Boltzmann carrier statistics, the total capacitance is equivalent for both accumulation and inversion regimes. What's more important is that the total capacitance for the three types of semiconductor is more elevated at Boltzmann statitics. In the Fig. 12 we appreciate the conduction band profile in a MIS capacitor with a three p-type substrate (Si, GaAs and InAs) for initial, medium and final applied bias to better understand the evolution of conduction band at different bias for the three different semiconductors and illustrate the band offsets for Al_2O_3 on each semiconductor. A quantum well appears in the interface Al_2O_3/semiconductor. In this spacious area the potential felt by a quantum particle reaches a minimum. This is a potential well in which small dimensions result in dissimilarity between the predictions of semi-classical mechanics and those of quantum mechanics. The progress of electrons and holes is then confined in a spatial direction and free in the other two directions (1D confinement). The movement of the carriers in the direction of confinement is discredited, resulting in energy bands shown in Fig. 6 and 7.

4. Conclusion

In summary, we theoretically investigate the differences between the semiclassical and quantum mechanical charge description at the interface Al_2O_3/Si-(100) orientation for Metal–Insulator–Semiconductor (MIS). At first, the use of the quantum model gives rise to a threshold voltage shift of about 100 mV, which is a significant and physically justified value. It is emphasized that during inversion region, there is about 10% degradation of the total gate capacitance when using the quantum mechanical model. We noticed that the difference between the semiclassical model and quantum model is clear only in the inversion zone and this is connected directly to the type of substrate doping and only the electrons are treated quantum mechanically. We studied a quantum confinement phenomenon quantization of energy carriers at discrete levels and their wave function with the distribution of carriers to the substrate surface. We notice that the minimum energy band in the quantum well whatsoever primed or unprimed ladder of subbands correspond with the highest amplitude wavefunction. The unprimed wavefunctions are more squeezed as the energies are lower and for those energies the well is squeezed. The very low effective density of state in the conduction band of III–V semiconductors is clearly evidenced in inversion regime, which leads to low capacitance values in $C-V$ characteristics for Fermi–Dirak carrier statitics. It should be noted that both the improved electrostatic control of the MIS compared to a DG, and the good transport properties of III–V materials due to their reduced effective masses, come at the expense of an increased variability of the shift between classical and quantum threshold voltages.

References

[1] T. Nguyen, C. Busseret, L. Militaru et al. Microelectron. Reliab., **47**, 4, 729 (2007).
[2] Xinlin Wang, Ting-wei Tang. J. Comput. Electron., **1**, (1-2), 283 (2002).
[3] F. Chirico, F. Della Sala, A. Di Carl et al. Phys. B: Condens. Matter, **272** (1), 546 (1999).
[4] Narain D. Arora. *MOSFET models for VLSI circuit simulation: theory and practice* (Springer Science & Business Media, 2012).
[5] Slah Hlali, Neila Hizem, Adel Kalboussi. J. Comput. Electron., **15** (4), 1340 (2016).
[6] International Roadmap Committee et al. International Technology Roadmap for Semiconductors, 2013, edition Executive Summary. Semiconductor Industry Association, San Francisco, CA, available at: http://www.itrs.Net/Links/2013ITRS/2013Chapters/2013ExecutiveSummary.pdf, 2013.
[7] N. Yang, W.K. Henson, J.R. Hauser. IEEE Trans. Electron Dev., **46**, 1464 (1979).
[8] J. Suné, P. Olivo, B. Riccó. IEEE Trans. Electron Dev., **39**, 1732 (1992).
[9] H. Carrillo-Nunez, A. Ziegler, M. Luisier et al. J. Appl. Phys. **117** (23), 234501 (2015).
[10] H. Carrillo-Nunez, A. Ziegler, M. Luisier et al. J. Appl. Phys., **117** (23), 234501 (2015).
[11] D. Vasileska, S.M. Goodnick, G. Klimeck. Computational Electronics: Semiclassical And Quantum Transport Modeling (2010).
[12] SCHRED version 2.1 USER MANUAL prepared by: Dragica Vasileska Arizona State University Tempe, AZ 85287-5706, USA.
[13] T. Nguyen. Caractérisation, modélisation et fiabilité des diélectriques de grille à base de hfo2 pour les futures technologies CMOS (2009). Thèse de doctorat. INSA de Lyon.
[14] K. Yang, Y.C. King, C. Hu et al. Proc. Symp. on VLSI Technology (1999) p. 77.
[15] Scott Hareland, M. Manassian, Wei-Kai Shih et al. IEEE Trans. Electron. Dev., **45** (7), 1487 (1998).
[16] Yang-Kyu Choi, Daewon Ha, Tsu-Jae King et al. *Threshold voltage shift by quantum confinement in ultra-thin body device*. In: *Device Research Conference*, 2001. IEEE (2001). P. 85.
[17] F. Li, S. Mudanai, L.F. Register et al. IEEE Trans. Electron Dev., **52**, 1148 (2005).
[18] Fei Li, S. Mudanai, Leonard Franklin et al. IEEE Trans. Electron. Dev., **52** (6), 1148 (2005).
[19] L. Farhang Matin, H. Hasan Bouzari, F. Ahmadi. J. Theor. Appl. Phys., **8** (3), 1 (2014).
[20] Mathieu Moreau, Daniela Munteanu, Jean-Luc Autran et al. *Quantum Simulation Of CV and IV Characteristics in Ge and III–V Materials/High-k Mos Devices*. In: *Mrs Proceedings* (Cambridge University Press, 2009). P. 1194-A02-02.
[21] J. Robertson, B. Falabretti. J. Appl. Phys., **100** (1), 4111 (2006).

Редактор K.V. Emtsev